Theoretical Kinetics Predictions for $NH_2 + HO_2$

Klippenstein, Stephen J.; Glarborg, Peter

Published in:
Combustion and Flame

Link to article, DOI:
10.1016/j.combustflame.2021.111787

Publication date:
2022

Document Version
Peer reviewed version

Theoretical Kinetics Predictions for $NH_2 + HO_2$

Stephen J. Klippenstein,[1] Peter Glarborg[2]

[1] Chemical Sciences and Engineering Division, Argonne National Laboratory, Lemont, IL 60439, USA
[2] DTU Chemical Engineering, Technical University of Denmark, 2800 Lyngby, Denmark
** Corresponding Author Email: sjk@anl.gov*

Abstract: Recent modeling studies of NH_3 oxidation, which are motivated by the prospective role of ammonia as a zero-carbon fuel, have indicated significant discrepancies between existing literature mechanisms. In this study high level theoretical kinetics predictions have been obtained for the reaction of NH_2 with HO_2, which has previously been highlighted as an important reaction with high sensitivity and high uncertainty. The potential energy surface is explored with coupled cluster calculations including large basis sets and high-level corrections to yield high accuracy (~0.2 kcal/mol) estimates of the stationary point energies. Variational transition state theory is used to predict the microcanonical rate constants, which are then incorporated in master equation treatments of the temperature and pressure dependent kinetics. For the radical-radical channels, the microcanonical rates are obtained from variable reaction coordinate transition state theory implementing directly evaluated multireference electronic energies. The analysis yields predictions for the total rate constant as well as the branching to the $NH_3 + O_2$, $H_2NO + OH$, and $HNO + H_2O$ channels. Rate constants are also reported for the $H_2NO + OH$ reaction as they arise naturally from the analysis. The rate constant and branching fraction determined in this work for the $NH_2 + HO_2$ reaction deviate significantly from values used in most previous modeling studies. The fact that the main product channel is chain terminating, rather than propagating, has strong implications for modeling NH_3 ignition and oxidation, in particular at intermediate temperatures and elevated pressure.

Keywords: *Theoretical Kinetics, NH_3 oxidation, Ab Initio Kinetics, NOx*

1. Introduction

Ammonia is a potential carbon-free energy carrier that has attracted a lot of attention recently [1-4]. Due to its poor combustion characteristics, its use in engines and gas turbines is expected to be quite challenging. Ammonia exhibits longer ignition delays and lower flame speeds than typical hydrocarbon fuels, emphasizing a need for reliable and versatile chemical kinetic models for design and optimization of appropriate combustion units.

The reactivity of ammonia is largely governed by the fate of the amino radical NH_2. At the high pressure and intermediate temperatures typical of ignition in compression ignition engines, the peroxy radical HO_2 is the main chain carrier and its reaction with NH_2:

$$NH_2 + HO_2 \rightarrow \text{products} \qquad \text{(R1)}$$

becomes a key step [5,6]. This reaction has several possible product channels:

$$NH_2 + HO_2 \rightarrow NH_3 + O_2 \qquad (\Delta H = -58.1 \text{ kcal/mol}) \qquad \text{(R1a)}$$
$$NH_2 + HO_2 \rightarrow HNO + H_2O \qquad (\Delta H = -79.8 \text{ kcal/mol}) \qquad \text{(R1b)}$$
$$NH_2 + HO_2 \rightarrow H_2NO + OH \qquad (\Delta H = -23.3 \text{ kcal/mol}) \qquad \text{(R1c)}$$
$$NH_2 + HO_2 \rightarrow NH_2OOH \qquad (\Delta H = -44.0 \text{ kcal/mol}) \qquad \text{(R1d)}$$

Ignition and oxidation of ammonia are affected by the overall rate constant for R1 and by its branching fraction. Of the two dominating products channels, $NH_3 + O_2$ (R1a) is chain terminating, while $H_2NO + OH$ (R1c) is propagating. The relative importance of these channels has a significant impact on the predicted reactivity of NH_3 at intermediate temperatures, but theoretical and experimental results are not conclusive.

Experimental results on the $NH_2 + HO_2$ reaction are limited to low temperature studies of NH_3/O_2 mixtures by either flash photolysis [7-21] or pulse radiolysis [22,23]. Much of the flash photolysis work were re-interpreted very recently by Glarborg et al. [24] using an updated detailed reaction mechanism [25]. Based on reported NH_2 decay rates in flash photolysis of $NH_3/O_2/N_2$ by Cheskis and Sarkisov [11], they derived a rate constant for $NH_2 + HO_2 \rightarrow NH_3 + O_2$ (R1a) of $k_{1a} = 1.5(\pm 0.5) \times 10^{14}$ cm^3 mol^{-1} s^{-1} at 295 K. This value is higher than the previous experimental determinations from the flash photolysis experiments (in the range (1.5-4.5) x 10^{13} cm^3 mol^{-1} s^{-1} [11, 13, 15, 16]) due to differences in the rate constants of important side reactions. Glarborg et al. also concluded that $NH_2 + HO_2 \rightarrow H_2NO + OH$ (R1c) was competing with R1a, but estimated an upper limit for this channel of 5x10^{13} cm^3 mol^{-1} s^{-1}, while the channel to $HNO + H_2O$ (R1b) was suspected to be minor.

Previous work on the $NH_2 + HO_2$ reaction also includes several theoretical studies [26-32]. Sumathi and Peyerimhoff [28] found that the dominant product channel was $NH_2O + OH$, formed from dissociation of an energized H_2NOOH adduct. Xian et al. [30] concluded that the reaction took place on both the singlet surface, yielding $H_2NO + OH$, and on the triplet surface, forming $NH_3 + O_2$. They were not able to determine the branching fraction, but indicated that reactions on the singlet surface possibly were dominating. In a recent study, Stagni et al. [32] calculated the rate constant for H-abstraction from NH_3 by O_2. Their value corresponds to a very fast rate constant

of 1.5 x 10^{14} cm^3 mol^{-1} s^{-1} at room temperature for the reverse step, $NH_2 + HO_2 \rightarrow NH_3 + O_2$ (R1a), in good agreement with the evaluation of Glarborg et al. [24]. The analysis of Stagni et al. was based on variational transition state theory implementing reasonably high-level energies (CCSD(T)/aug-cc-pVTZ//M06-2X/aug-cc-pVTZ). Thus, it should provide a reasonably satisfactory prediction of the temperature dependence of this channel. However, Stagni et al. did not address the importance of the other product channels for $NH_2 + HO_2$.

The theoretical studies of Sumathi et al. [28], Tiancheng et al. [29], and Mousavipour et al. [31] each provide detailed examinations of the potential energy surfaces of relevance to the reaction of NH_2 with HO_2. The stationary point energies were explored with similar methods in these studies; QCISD(T)/6-311+G(2df,2pd)//MP2/6-311++G**, CCSD(T)/6-311++G(3df,3pd)//B3LYP/6-311++G(3df,3pd), and CCSD(T)/aug-cc-pVTZ//MPW1K/6-31+G(d,p), respectively. Qualitatively, one expects 2σ uncertainties for these methods of about 3 kcal/mol.

While the studies of Mousavipour et al. and Sumathi et al. also predict the thermal rate coefficients, limitations in their methodologies studies suggest that their predicted rate constants are unlikely to be quantitatively accurate. In particular, both the entrance and primary exit channel (1c) for the reaction on the singlet state are radical-radical in nature. Correspondingly, quantitative predictions for these channels [which are the primary bottlenecks for the overall singlet reaction and the branching to channel (1c), respectively] require the use of multireference based explorations of the energetics. Furthermore, variational effects would be expected to have a significant impact on the predicted kinetics (i.e., more than a factor of two) for such channels. Sumathi et al. simply presume a rate constant of 2.5 x 10^{13} cm^3 mol^{-1} s^{-1} for the entrance channel, while their treatment of the exit channel is qualitative in nature. Mousavipour et al. consider both ab initio transition state theory-based master equation and quasiclassical trajectory analyses. However, since they make no mention of how they treat the barrierless channels, and make no reference to either multireference electronic structure methods or variational transition state theory, their estimated rate constants cannot be expected to be reliable.

Accurate rate constants for $NH_2 + HO_2$ as a function of temperature and pressure are required for reliable prediction of ammonia ignition and oxidation under conditions of engines and gas turbines, i.e., elevated pressure and intermediate temperatures [5,6]. In this work, we employ a combination of high-level electronic structure theory and sophisticated variational transition state theory methods to obtain high quality predictions for the rate constants for all product channels. The radical-radical channels are each treated with variable reaction coordinate transition state theory, which has generally agreed with experimental observations to within about 20% in prior studies [33]. The stationary point energies are treated with a modestly improved version of the ANL0 method [34], which employs a CCSD(T)/CBS analysis combined with a variety of additional corrections to obtain 2σ uncertainties of ~ 0.2 kcal/mol.

We also examine the pressure dependence of the $NH_2 + HO_2$ kinetics through master equation simulations for pressures up to 100 atm, but find little indication of stabilization or pressure dependence for the kinetics. Nevertheless, this master equation analysis also yields predicted rate constants for the reaction of H_2NO with OH, which do indicate some stabilization of the NH_2OOH complex at higher pressures. For completeness, the predicted rate coefficients for the reactions

starting from H_2NO + OH are also reported here. The implications of the updated NH_2 + HO_2 rate coefficients for NH_3 modeling predictions are discussed.

2. Methods

2.1 Stationary Points on the Potential Energy Surface

Initial explorations of the stationary points with a variety of density functional theory (DFT) and coupled cluster methods found significant differences between the optimized structures at different levels of theory. Thus, coupled cluster methods, which are generally more reliable than DFT, were used to optimize the geometries. Notably, calculations at the CCSD(T)/cc-pVTZ level were found to deviate from the complete basis set (CBS) limit by more than 5 kcal/mol for one species ($OHNH_2O$), and 2-4 kcal/mol for a number of other structures. Such large deviations from the CBS limit can correlate with significant errors in the optimized geometries and correspondingly the predicted energies and vibrational properties. Thus, we also explored the use of the explicitly correlated CCSD(T)-F12 method [35] to predict the stationary point geometries. This method tends to yield energies that are close to the CBS limit even with relatively modest basis sets and at only modestly increased cost. Furthermore, we find that this method generally yields markedly improved frequency estimates. For the NH_2 + HO_2 system, we find that our results for the cc-pVDZ-F12 and cc-pVTZ-F12 basis sets [36] are indeed significantly more reliable, with maximum deviations from the CBS limit of 0.7 and 0.5 kcal/mol, respectively. Furthermore, typical deviations were less than 0.2 kcal/mol. Thus, the results reported here are based on optimized geometries and vibrational frequencies obtained at the CCSD(T)-F12/cc-pVTZ-F12 level.

Complete basis set (CBS) limit estimates for the vibrational zero-point energies were obtained via extrapolation of CCSD(T)-F12 values for the cc-pVDZ-F12 and cc-pVTZ-F12 basis sets. Meanwhile, higher accuracy estimates for the stationary point energies were obtained from a composite approach incorporating (i) CCSD(T)-F12 estimates for the CBS limit based on explicit calculations for the cc-pVTZ-F12 and cc-pVQZ-F12 basis sets, (ii) CCSDT(Q)/cc-pVDZ corrections for the effect of higher order excitations, (iii) CCSD(T)/CBS calculations of core-valence effects based on extrapolations of results for the cc-pcVTZ and cc-pcVQZ basis sets [37], (iv) CCSD(T)/aug-cc-pcVTZ-DK calculations of scalar relativistic effects employing the Douglas-Kroll-Hess (DKROLL=1) one electron integrals [38], (v) HF/cc-pVTZ evaluations of the diagonal Born-Oppenheimer correction (DBOC), and (vi) B2PLYP-D3/cc-pVTZ [39] based calculations of anharmonic vibrational corrections through second order vibrational perturbation theory.

The CBS extrapolations employed coefficients of 0.5 and 0.4 for the CCSD(T)-F12 energy and frequency extrapolation, respectively, and 0.69 for the core-valence energies. The results are only very weakly dependent on reasonable values for the extrapolation coefficients (i.e., there is an extrapolation uncertainty of a few hundredths of a kcal/mol typically). Complete basis set limit CCSD(T) energies were also obtained from calculations for the aug-cc-pVQZ′ and aug-cc-pV5Z′ basis sets, with a maximum difference from the CCSD(T)-F12/CBS limit of 0.08 kcal/mol. Here, the CCSD(T)/aug-cc-pVnZ′ extrapolations involve larger extrapolations from the explicit value for the largest basis set than do the CCSD(T)-F12/cc-pVnZ-F12 extrapolations. Thus, we have chosen to use the CCSD(T)-F12/CBS limits for the present kinetic analyses.

The calculations were mostly performed with MOLPRO [40,41]. The evaluations of the DBOC, were performed with CFOUR, as were the CCSDT(Q) calculations for singlet states [42]. For doublet and triplet states, the CCSDT(Q) calculations employed Kallay's MRCC extension to MOLPRO [43]. The anharmonicity corrections were obtained with GAUSSIAN [44]. The coupled cluster calculations employ a restricted spin Hartree-Fock wavefunction within the unrestricted coupled cluster formalism, except for the CCSDT(Q) calculations which employ an unrestricted spin wavefunction for both the HF and coupled-cluster components. The CCSDT(Q) correction was then taken as the difference between the UUCCSDT(Q)/cc-pVDZ result and the RUCCSD(T)/cc-pVDZ result.

The present analysis, which we label here as ANL0F, represents a modest improvement over the related ANL0 methods through the use of the more accurate CCSD(T)-F12/cc-pVTZ-F12 geometries and harmonic frequencies. Thus, we expect the final energy estimates to have similar or lower 2σ uncertainties of 0.2 kcal/mol for the minima. The expected uncertainties for ANL0F predictions of the saddlepoints are less clear, but our experience from more limited comparisons suggests that these energies typically have similar uncertainties, at least when the T(Q) correction is not too large (i.e., less than 1 kcal/mol). For example, we have recently made a detailed comparison of a related calculation of the dissociation kinetics for the QOOH arising from t-butyl oxidation with time-resolved experimental measurements [45]. These results agree with experiment to within about 20% with no adjustment in the barrier height, as have as numerous of our related calculations for H transfer induced dissociations of Criegee intermediates [46]. Other calculations for various addition and abstraction reactions of combustion and astrochemical relevance (See, e.g., [47-49]) show similar agreement. In short, every time we have had definitive experimental data for comparison, we find that the errors attributable to the barrier heights are on the order of 0.2 kcal/mol or less. It is perhaps worth noting though that coming to such conclusions via comparison with experiment requires careful analysis of variational, anharmonicity, and tunneling effects, as well as the use of a high-level method to locate the saddle point.

This finding goes against conventional wisdom that transition states have more complex wavefunctions and thus their predictions should be more inaccurate. The satisfactory agreement we find is likely indicative of the fact that the CCSDT(Q) correction is generally able to capture the key multireference effects in wavefunctions, as long as the correction is not too large [34]. This statement appears to hold just as well for transition states as for stable structures. When the T(Q) correction is large, we would instead resort to multireference methods, as we do for the radical-radical channels here. It is perhaps also worth noting that the evaluations of barrier heights typically involves less chemical change than the evaluation of the heat of formation from atoms or small molecules (as was common practice). Of course, the use of isodesmic reactions ameliorates those problems for heats of formation, but then introduces a coupling to experimental measures for the reference reaction.

2.2 Radical-Radical Interactions

The NH_2 + HO_2 entrance channel and OO fission exit channel from NH_2OOH involve the interaction of two radicals. The interaction energies for such radical-radical channels in their low spin state cannot be treated effectively with standard single reference methods such as CCSD(T). Instead, we employ the complete active space second order perturbation theory (CASPT2) and

Davidson corrected multireference singles and doubles configuration interaction (MRCI+QC) methods. The energies from these multireference calculations need to be tied back to the energy framework for the overall system. Here, this is accomplished by using the multireference methods to calculate the energies relative to either separated fragments (NH_2 + HO_2 or H_2NO + OH) or the triplet states at the same geometry. The latter approach is particularly effective because multireference methods are more consistent (and likely more accurate) in their prediction of these spin-splittings than in their prediction of the interaction energies relative to separated fragments. However, this spin-splitting approach requires additional high-level calculations of the triplet state energies, and so we only implement it when deemed necessary, as indicated by significant differences between the CASPT2 and MRCI+QC analyses.

Radical-radical reactions generally involve multiple transition states describing various large amplitude motions through the long-range portion of the potential energy surface where the chemical interactions are quite weak. For the NH_2 + HO_2 and H_2NO + OH reaction channels, hydrogen-bonded van der Waals (vdW) complexes (here labelled NH_2…HO_2 and H_2NO…OH, respectively) mediate the transition from long-range interactions to chemical interactions (cf. Fig. 1 for the NH_2…HO_2 case). In the region of these long-range complexes, the singlet and triplet states are nearly degenerate, and are likely strongly coupled. For the H_2NO…OH case, there are also two possible orientations of the OH radical orbital, which creates an additional set of nearly degenerate states for both the singlet and triplet states in the vdW region.

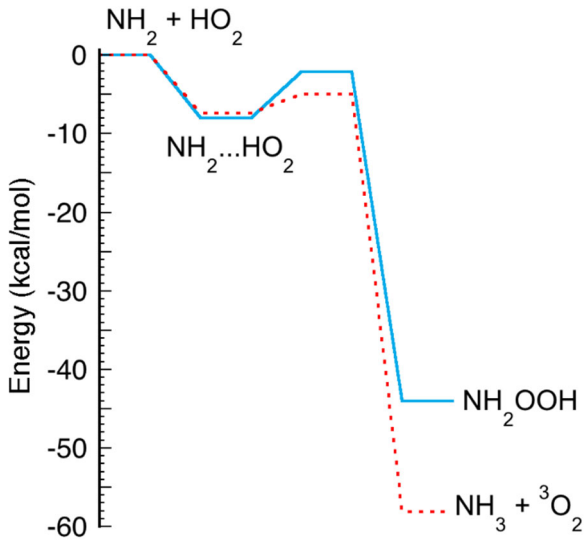

Fig. 1. Schematic plot of the entrance channel PES for the reaction of NH_2 with HO_2. The solid blue line denotes the singlet state, while the dashed red line denotes the triplet state. The triplet state energies are from ANL0F calculations, while singlet state energies are from CASPT2/CBS//CASPT2/cc-pVTZ-F12 calculations.

Here, we implement the variable reaction coordinate transition state theory to treat these channels [50,51]. This approach has been found to yield high accuracy a priori rate predictions when sufficient attention is paid to the generation of accurate interaction energies [52]. Here we employ direct sampling of multireference (CASPT2 or MRCI+QC) energies in the underlying phase space integrals. We also include one-dimensional corrections to these interaction energies obtained from

higher level analyses and including effects for geometric relaxation along the reaction path. Separate treatments are employed for each of the various different reaction channels.

The evaluation of the one-dimensional corrections begins with a sequence of constrained optimizations, followed by higher accuracy calculations at the optimized constrained geometries. For the NH_2 + HO_2 reaction, the NO distance was constrained at various values, while the other coordinates were fully optimized at the CASPT2(2e,2o)/cc-pVTZ level. The two orbitals for the active space correlate with the radical orbitals of the separated fragments. A relaxation correction is obtained from related optimizations where the internal structures of the NH_2 and HO_2 are also constrained. These constrained internal structures are used in the orientational sampling in the VRC-TST calculations. Higher accuracy energies are obtained from CASPT2 calculations for the cc-pVQZ and cc-pV5Z basis sets, which are then extrapolated to the CBS limit with an extrapolation coefficient of 0.93. Notably, for this channel the sum of the relaxation and higher accuracy corrections is less than 15 % of the CASPT2/cc-pVTZ constrained geometry energy. Qualitatively, when this correction is small one expects the direct rigid body plus one-dimensional corrections approach to be reliable. Thus, we expect that the present CASPT2/cc-pVTZ based direct sampling VRC-TST approach should yield high accuracy rate estimates.

As illustrated in Fig. 2, related MRCI+QC/CBS and CASPT2/CBS calculations of the interaction energies (relative to separated NH_2 + HO_2) along the CASPT2/cc-pVTZ distinguished coordinate minimum energy path differ by 10% or less in the key transition state region (from 2.5 Å down to about 2 Å). Including an IPEA shift [53] in the CASPT2 calculations yields a similar deviation from the CASPT2/CBS minimum energy path (cf. Fig. 2). With this small difference between the three methods, the implementation of a spin-splitting based approach was deemed unnecessary for the NH_2 + HO_2 channel.

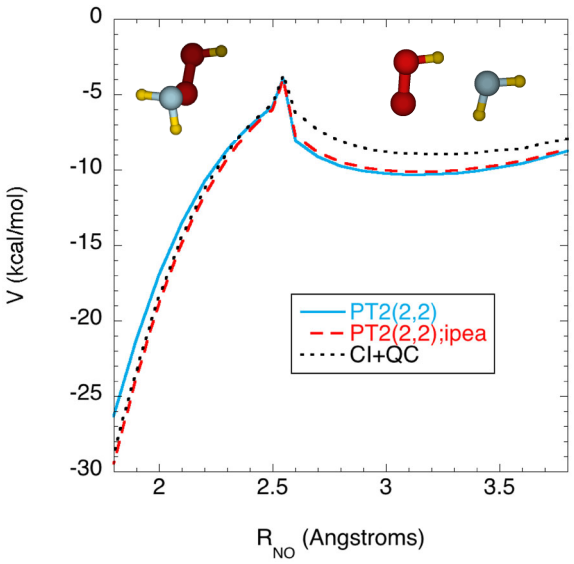

Fig. 2: Schematic plot of the interaction between NH_2 and HO_2 on the singlet PES in the region of the transition state for formation of NH_2OOH. The solid blue, dashed red, and dotted black lines denote the CASPT2/CBS with and without the IPEA shift, and the MRCI+QC/CBS results,

respectively. All calculations employ the geometries from distinguished coordinate optimizations at the CASPT2/cc-pVTZ level.

Note that the spike in the plot near the saddle point arises because of a distinctly different orientation of the NH_2 and HO_2 groups for small and large NO separations. In essence, the saddle point corresponds to rotation from the optimum hydrogen bonding orientation to the optimum chemical bonding orientation (cf. structures in the Fig. 2 insets). However, the actual inner transition state (i.e., the location of the minimum in the flux bottleneck) occurs at even shorter separations (e.g., 2.4 to 2.0 Å) where the chemical bond is starting to form. There is also a longer-ranged transition state (e.g., for separations of 4-6 Å) corresponding to formation of the NH_2…OOH complex.

For the NH_2 + HO_2 entrance channel, the present kinetic analysis considers three distinct transition states. First, a VRC-TST calculation is performed to predict the reactive flux proceeding from the separated reactants into the vdW regime. The reaction coordinate is presumed to be the separation between the two centers-of-mass (ranging from 20 to 7 bohr) and the CASPT2/cc-pVTZ method is used in the direct sampling over orientations. These calculations begin by explicitly evaluating the flux for addition on the singlet state. The overall flux to the vdW regime is then taken as the sum of singlet and triplet fluxes with the triplet flux assumed to be three times the singlet flux. This assumption presumes that the intersystem crossing between the triplet and singlet states if rapid, which seems reasonable given that the CASPT2/CBS predicted splitting at the long-range minimum is just 0.02 kcal/mol. Importantly, this assumption has essentially no bearing on the rate predictions at combustion temperatures, where the main bottlenecks occur after the formation of the vdW complexes.

The flux for proceeding from the NH_2…HO_2 vdW complex onto NH_2OOH (the singlet inner transition state) is evaluated with a separate VRC-TST analysis, again employing direct CASPT2/cc-pVTZ energies. For this inner transition state, the reaction is presumed to proceed on only the singlet surface. The reaction coordinate is taken to be the distance between pivots (ranging from 8 to 3.75 bohr), with two pivot points on each radical. For NH_2, these two pivot points are located along the radical orbitals; i.e., displaced directly above and below the NH_2 plane atop the N atom by 0.5 bohr. A similar pivot point displacement along the terminal O radical orbitals is employed for the HO_2 pivot points with displacements of 0.01, 0.5, and 1 bohr.

This different choice of reaction coordinates for the outer and inner transition state regions is related to the fact that in the outer transition state region chemical bonding is insignificant, and so a center-of-mass reaction coordinate is most appropriate, whereas in the inner transition state region chemical bonding yields a sharp drop in the interaction potential along the minimum energy path and so radical-orbital to radical-orbital separations determine the reaction coordinate. For all of the present VRC-TST calculations, the number of sampling points is chosen to yield convergence of the phase space integrals to +/- 5% at the 1σ level. The pivot point locations and separations are expected to yield a similar level of convergence for the dividing surface minimization within the VRC-TST approach. For each of these VRC-TST calculations we append a dynamical recrossing correction factor of 0.85 in keeping with the expectations from dynamical simulations for simple model systems [54].

The abstraction reaction to produce NH_3 + $^3O_2$ proceeds from the triplet vdW complex. Importantly, for the high-spin triplet state, single reference based methods methodologies are generally appropriate. Thus, the triplet abstraction saddle point properties were evaluated at the ANL0F level. Variational transition state theory was then implemented by following the steepest descent path. This path and the corresponding energies and transverse frequencies along it were all evaluated at the CCSD(T)-F12/cc-pVDZ-F12 level. A step size of 0.1 was used for this analysis, with calculations for a five times smaller step deviating by less than 1%. The OONH torsional motions for this transition state were treated as a one-dimensional hindered rotor, with the torsional potential designed to reproduce the torsional frequency for the C1 saddle point as well as the energies of the cis and trans second order saddle points. The torsional potentials along the minimum energy path were obtained by scaling according to the square of the ratio of the path dependent harmonic torsional frequencies. The overall triplet state abstraction rate constant is by the combination of the bottleneck to form the vdW complex (determined as described above) and this inner transition state for the triplet state.

For completeness, we also briefly explored the triplet abstraction $NH_2 + HO_2 \rightarrow {}^3NH + H_2O_2$ and the singlet abstraction $NH_2 + HO_2 \rightarrow NH_3 + {}^1O_2$. The former channel is 6.2 kcal/mol endothermic with a barrier of about 16.0 kcal/mol, and so is not expected to be significant. Obtaining accurate predictions for the latter channel is challenging due to the presence of significant multireference effects in $^1O_2$. Predicted barrier heights of 4.5 and 5.5 kcal/mol, were obtained for CI+QC(4,4)/cc-pVTZ and PT2(12,11)/cc-pVTZ methods, respectively. For the former barrier, the rate constant for producing NH_3 + $^1O_2$ is predicted to be <1% of the total $NH_2 + HO_2$ rate constant for T < 2000 K with $k = 1.87 \times 10^{-3}\ T^{4.14} \exp(3340/RT)$ $cm^3\ mole^{-1}\ s^{-1}$.

The potential energy surface for the interaction of H_2NO with OH is even more complex. The orbital degeneracy in the OH radical yields two nearly degenerate singlet states in addition to two nearly degenerate triplet states in the long-range/vdW region of the interaction. Furthermore, from these vdW complexes, the OH can add to either the O end of H_2NO (to form NH_2OOH) or the N end (to form $OHNH_2O$). Here we employ three separate VRC-TST analyses to evaluate the reactive flux for forming the vdW complexes and for proceeding from the vdW complex on to either of the two chemical adducts.

Due to certain difficulties with the PT2 approach related to the near planarity of the umbrella mode in the H_2NO radical we employ the MRCI+QC(2,2)/cc-pVTZ method for our direct orientational sampling in these channels. One dimensional corrections are again obtained from evaluations of the geometry relaxation energy and MRCI+QC/CBS(QZ,5Z) evaluations along distinguished coordinate minimum energy paths. For the addition to form NH_2OOH, the pivot points for the NH_2O fragment were displaced above and below the O atom (by 0.01, 0.5, and 1 bohr), while for the addition to form $OHNH_2O$ they were displaced above and below the N atom (by 0.01, 0.5, and 1 bohr). The OH pivot point was taken to be at its center-of-mass. The addition to the O and N ends of H_2NO were separated according to whichever distance was smaller during the orientational sampling. Pivot point separations ranging from 8 to 3.5 bohr were considered. The reaction coordinate was presumed to be the center-of-mass separation distance for the vdW formation process. Estimated dynamical correction factors of 0.85 were again employed in the final rate predictions.

Notably, prior studies have suggested that there is also a tight transition state for producing $OHNH_2O$ from H_2NOOH. For example, in Ref. [30] this transition state was predicted to lie 3 kcal/mol above the threshold for forming $H_2NO + OH$. Our attempts to locate this transition state with coupled cluster calculations were unsuccessful. Further analysis employing multireference methods and fixed separation angular scans indicated that this saddle point is specious. This tight transition state instead merges smoothly into a roaming transition state that provides the transition between the two chemical adducts at long range. The failure of the prior calculations is a result of the limitation of closed shell methods in describing diradical states. In essence, the OO separation of 2.1 Å for the TS in the B3LYP calculations from [30] is so large that a diradical is being formed, and single-reference based methods are no longer effective.

2.3 Thermal Rate Constants

The full-temperature and pressure dependence of the rate constants were estimated through the implementation of these microcanonical rates into the master equation employing the MESS master equation solver [55]. The torsional modes for NH_2OOH and $OHNH_2O$ were treated as one-dimensional hindered rotors with the torsional potentials mapped at the CCSD(T)-F12/cc-pVTZ-F12 level. Asymmetric Eckart tunneling corrections were included for all the tight transition states. The energy transfer was represented with Lennard Jones collisions rates and a temperature dependent [$<\Delta E_{down}> = 100\ (T/298)^{0.85}$] exponential down formula and the bath gas was taken to be N_2. For the $NH_2 + HO_2$ reaction, these master equation calculations indicate essentially no pressure dependence up to 300 atm.

3. Results and Discussion

Potential Energy Surface

The components of the present calculations of the stationary point energies on the NH_3O_2 potential energy surface are provided in Tables 1 through 3 and illustrated schematically in Fig. 3. The energetics are compared with those from prior studies in Table 4.

The results reported in Table 1 provide some indication of the expected accuracy of the final predictions for the various stationary point energies. The small differences between the CCSD(T)-F12 for the CBS limit and the cc-pVQZ-F12 values indicates that are all the results are well converged with respect to the basis set. The average absolute values of the CCSDT(Q)/cc-pVDZ, core-valence, relativistic, DBOC, and anharmonic corrections are 0.57, 0.22, 0.11, 0.11, and 0.14 kcal/mol, respectively. Clearly, the CCSDT(Q) correction is of considerable importance to making accurate predictions of the kinetics.

The saddle point for the triplet abstraction (R1a) has a fairly large T1 diagnostic of 0.050, which is often indicative of significant multireference effects. This indication is further reflected in the large value of -0.83 kcal/mol for the CCSDT(Q) correction. From our experience, we expect that this CCSDT(Q) correction captures the majority of the multireference effects. Nevertheless, its large magnitude does indicate an increased uncertainty in the predicted saddle point energy; perhaps it is about 0.4 kcal/mol. Notably, the CCSDT(Q) corrections for the two conformers of the $OHNH_2O = HNO + H_2O$ saddle point are each -1.9 kcal/mol. For such large corrections, it is

unlikely that the multireference effects are accurately captured. Correspondingly, the uncertainty in that saddle point energy is perhaps 2 kcal/mol. Fortunately, the predicted kinetics is only weakly dependent on that energy.

The H_2NO radical is only weakly nonplanar. As a result, the anharmonic correction for this radical is larger than normal. There is a correspondingly larger uncertainty in its zero-point energy, and the uncertainty in the total energy is then perhaps 0.3 kcal/mol. For all other stationary points, we expect a 2σ uncertainty in the total energy relative to $NH_2 + HO_2$ of about 0.2 kcal/mol.

Table 1: Components of the ANL0F energies (kcal/mol) for the stationary points on the potential energy surface for NH_2 reacting with HO_2. All are relative to $NH_2 + HO_2$.

Stationary Point	CCSD(T)-F12 QZ-F12	CBS	T(Q) DZ	CV CBS	Rel.	DBOC	E0 har	anh	T1 Diag	Total
					Minima					
$NH_2 + HO_2$	0	0	0	0	0	0	0	0	0.037	0
$^3NH_2…HO_2$	-9.45	-9.46	-0.05	-0.07	0.04	-0.05	2.37	-0.13	0.032	-7.36
$NH_3 + O_2$	-60.40	-60.38	-0.16	-0.30	0.01	-0.16	2.95	-0.05	0.008	-58.08
NH_2OOH	-49.77	-49.88	-0.06	-0.14	0.12	-0.17	6.30	-0.16	0.015	-44.00
$OHNH_2O$	-61.09	-61.24	0.06	-0.23	0.23	-0.17	7.57	-0.19	0.030	-53.98
$^3H_2NO…OH$	-31.50	-31.53	0.34	-0.42	0.16	-0.06	1.25		0.023	-28.22
$H_2NO + OH$	-24.04	-24.06	0.40	-0.39	0.14	-0.09	1.25	-0.46	0.030	-23.32
$HNO + H_2O$	-80.75	-80.81	-0.03	-0.20	0.12	-0.08	1.28	-0.03	0.016	-79.76
					Saddle Points					
$^3NH_2…HO_2 = NH_3 + {}^3O_2$	-3.81	-3.79	-0.83	-0.06	0.01	-0.02	0.42		0.050	-5.02
$OHNH_2O = HNO+H_2O$; geoa	-42.88	-42.93	-1.87	-0.19	0.15	-0.16	3.61	-0.05	0.030	-41.45
$OHNH_2O = HNO+H_2O$; geob	-40.36	-40.42	-1.91	-0.19	0.14	-0.15	3.55	-0.08	0.030	-39.06

The multireference predictions for the $NH_2…HO_2$ stationary point energies provided in Table 2 again show a good convergence with respect to basis set. For the $NH_2…HO_2$ minima the CASPT2-F12 and MRCI+QC-F12 results differ by 1.4 kcal/mol. For the $^3NH_2…HO_2$ minimum the CASPT2-F12 result agrees well with the ANL0F value provided in Table 1, which indicates that in this region of configuration space, the CASPT2-F12 method provides a better treatment of $NH_2…HO_2$ interactions. There is a submerged saddle point for the conversion from the $NH_2…HO_2$ vdW minimum to the NH_2OOH complex. This saddle point correlates with a reorientation from the optimal long-range orientation to that needed for chemical bond complex. Notably, variational reductions in the reactive flux at shorter separations significantly reduce the predicted rate constant.

Table 2: Multireference energies (kcal/mol) for the interaction of NH_2 with HO_2.[a]

Stationary Point	PT2-F12 TZ-F12	CBS	CI-F12+QC TZ-F12	CBS	E0[b] har	Total[c]
$NH_2 + HO_2$[d]	0	0	0	0	0	0
$^3NH_2…HO_2$	-10.0	-10.0	-8.6	-8.6	2.4	-7.6
$^1NH_2…HO_2$	-10.1	-10.0	-8.7	-8.6	2.4	-7.6

$NH_2…HO_2 = NH_2OOH$	-3.9	-3.9	-3.7	-3.7	1.9	-2.1

[a] All are at the PT2-F12(2,2)/cc-pVTZ-F12 geometries and are relative to $NH_2 + HO_2$.
[b] Relative zero-point energy (ZPE) from PT2-F12(2,2)/cc-pVTZ-F12 calculations.
[c] Sum of the PT2-F12/CBS energies and the PT2-F12/cc-pVTZ-F12 ZPE.

For the interaction of OH with NH_2O the MRCI+QC-F12 results are again well converged with respect to basis set (cf. Table 3). As expected, the calculations indicate submerged saddle points for the transition from a singlet vdW complex to either the NH_2OOH or the $OHNH_2O$ chemical complex. The MRCI+QC-F12 predicted singlet vdW energy of -4.8 kcal/mol is close to the ANLF0 predicted triplet vdW energy of -4.90 kcal/mol, indicating again a near degeneracy of singlet and triplet states in the vdW region.

Table 3: Multireference energies (kcal/mol) for the interaction of OH with NH_2O.[a]

Stationary Point	CI-F12+QC DZ-F12	CI-F12+QC TZ-F12	E0[b] har	Total[c]
$H_2NO + OH$	0	0	0	0
$NH_2OOH = H_2NO…OH$	-4.5	-4.5	1.5	-2.8
$H_2NO…OH$	-7.2	-7.2	2.2	-4.8
$H_2NO…OH = OHNH_2O$	-5.1	-5.1	1.8	-3.1

[a] All are relative to $NH_2O + OH$.
[b] Relative ZPE from CI-F12+QC(2,2)/cc-pVTZ-F12 calculations.
[c] Sum of the CI-F12+QC(2,2)/cc-pVTZ-F12 energy and ZPE, and the relative spin-orbit energy.

The schematic plot of the energies (Fig. 3) shows that the highest saddle point for the triplet reaction pathway lies somewhat lower in energy than that for the singlet pathway. For the singlet pathway, the transformation from NH_2OOH to $OHNH_2O$ occurs through a roaming radical process. That is, there is first a partial fission of the OO bond to form an $H_2NO…OH$ vdW complex, followed by a reorientation of the OH fragment relative to the H_2NO one, which leads directly to the $OHNH_2O$ chemical complex. Interestingly, the two saddle points involved in this roaming process lie at essentially the same energy. However, as is common for roaming radical processes, the continued fission of the $H_2NO…OH$ complex is expected to rapidly dominate over the roaming kinetics once the available energy exceeds the fission threshold. Our multireference calculations indicate that there is no saddle point for the direct transfer of the OH group from the O to the N at short separations. Once formed, the $OHNH_2O$ complex should rapidly dissociate to $HNO + H_2O$.

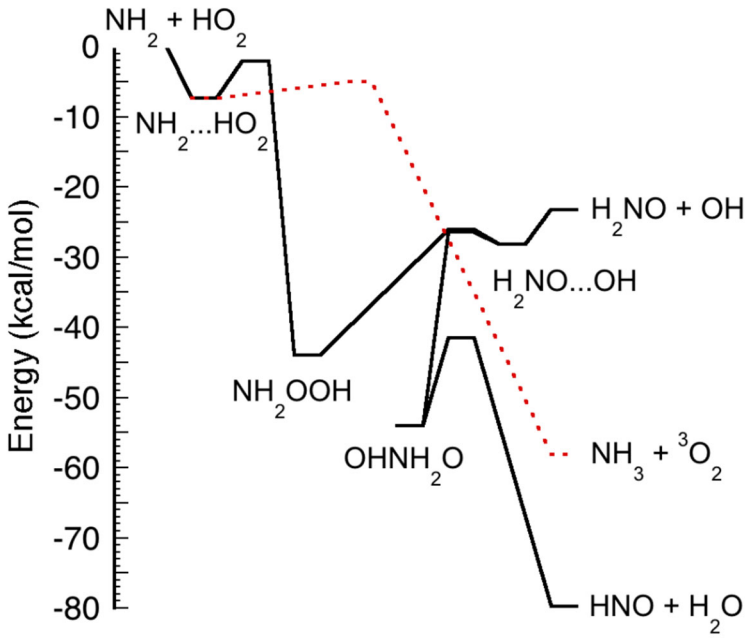

Fig. 3. Schematic plot of the reaction path energies (ANL0F and MRCI+QC) for the reaction of NH_2 with HO_2. The dotted red line denotes the triplet abstraction reaction path, while the solid black lines denote pathways on the singlet electronic surface.

Table 4: Comparison of the present best estimate zero-point corrected stationary point energies with literature values (kcal/mol).

Stationary Point	Present Work	Sumathi[a] QCISD(T) 6-311+G(2df,2pd)	Tiancheng[b] CCSD(T) 6-311++G(3df,3pd)	Mousavipour[c] CCSD(T) aug-cc-pVTZ	Stagni[d] CCSD(T) aTZ
Minima					
$NH_2 + HO_2$	0	0	0	0	0
$^3NH_2…HO_2$	-7.36	-	-7.4	-11.7	-
$NH_3 + O_2$	-58.08	-	-57.0	-	-57.1
NH_2OOH	-44.00	-41.7	-41.7	-41.0	-
$OHNH_2O$	-53.98	-51.9	-52.0	-51.0	-
$^3H_2NO…OH$	-28.22	-	-	-	-
$H_2NO + OH$	-23.32	-	-23.4	-22.2	-
$HNO + H_2O$	-79.76	-78.9	-79.2	-76.9	-
Saddle Points					
$^3NH_2…HO_2 = NH_3 + O_2$	-5.01	-	-6.2	-0.5	-4.2
$^1NH_2…HO_2 = NH_3 + {}^1O_2$	4.5				
$NH_2…HO_2 = NH_2OOH$	-3.2	-	-	-	-
$NH_2OOH = OHNH_2O$		-19.7	-20.6	-34.3	-
$OHNH_2O = HNO + H_2O$	-41.45	-35.9	-38.2	-37.6	-
$NH_2OOH = H_2NO…OH$	-26.1	-	-	-	-
$OHNH_2O = H_2NO…OH$	-26.4	-	-	-	-

[a] From [28]. [b] From [30]. [c] From [31]. [d] From [32].

The present energetic predictions differ by as much as 5.5, 3.2, 4.5, and 1.0 kcal/mol from those presented in [28], [30], [31], [32], and respectively. Such differences are not unexpected for the levels of theory employed in these previous works.

Rate Predictions

The present predictions for the rate constants (cm^3 $mole^{-1}$ s^{-1}) are well reproduced over the 300-2500 K range by the expressions:

$6.04x10^{18}$ $T^{-1.91}$ exp(-306/RT) + $5.91x10^{7}T^{1.59}$ exp(1373/RT)	(R1a)
$1.02x10^{12}$ $T^{0.166}$ exp(938/RT)	(R1b)
$2.19x10^{9}$ $T^{0.791}$ exp(1428/RT)	(R1c)
$2.14x10^{15}$ $T^{-0.751}$ exp(464/RT)	$H_2NO+OH = HNO+H_2O$
$6.07x10^{24}$ $T^{-5.64}$ exp(-1366/RT)	$H_2NO+OH = NH_2OOH$; 0.1 bar
$3.37x10^{26}$ $T^{-5.84}$ exp(-1303/RT)	$H_2NO+OH = NH_2OOH$; 1 bar
$2.18x10^{28}$ $T^{-6.07}$ exp(-1528/RT)	$H_2NO+OH = NH_2OOH$; 10 bar
$1.98x10^{29}$ $T^{-6.02}$ exp(-1930/RT)	$H_2NO+OH = NH_2OOH$; 100 bar
$1.48x10^{29}$ $T^{-5.82}$ exp(-2121/RT)	$H_2NO+OH = NH_2OOH$; 300 bar

for R in cal mol^{-1} K^{-1}. Note that the rate expression for the $H_2NO + OH = NH_2OOH$ reaction at 300 bar may be of limited validity due to the effect of non-binary collisions.

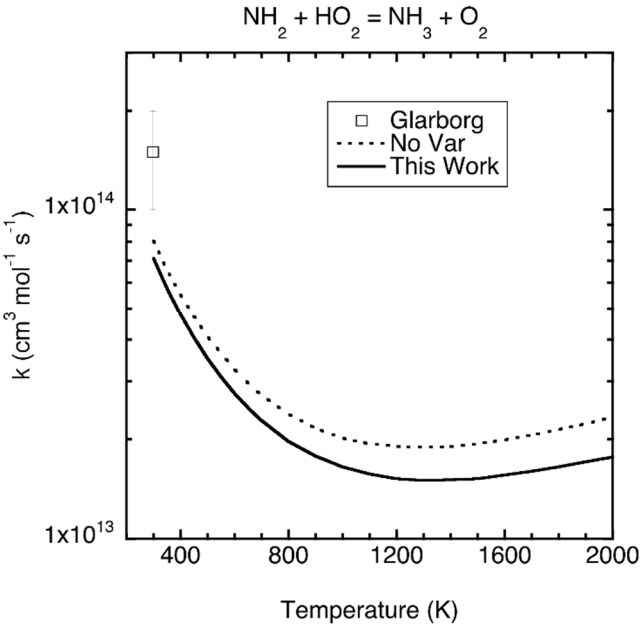

Fig. 4. Plot of the temperature dependence of the predicted rate constant for reaction (R1a). The experimental data is from [24]. The solid and dashed lines are for the present theoretical treatments with and without the inclusion of a variational treatment of the inner transition state of the triplet state.

As shown in Fig. 4, the predicted rate constant for (R1a) is about two times smaller than the value extracted from the recent reanalysis of flash photolysis data by Glarborg et al. [24]. This

discrepancy seems reasonable given the uncertainties in both that reanalysis and the present theoretical analysis. The dashed line illustrates that the variational effect for the inner transition state of the triplet state is quite small. It gradually increases from a 12% reduction to a 24% reduction from 300 to 2000 K. The variational effect arising from this channel, which is primarily due to a 0.3 kcal/mol shift in the barrier height at the zero-point corrected saddlepoint, is partly muted by the fact that the bottleneck for forming the vdW complex is the dominant bottleneck at low T.

It is interesting to consider the effect of variations in the theoretical parameters on the rate predictions for R1a. Decreasing the triplet abstraction saddle point energy (and corresponding minimum energy path energies) by 0.5 kcal/mol yields at most a 27% increase in the R1a rate constant. Artificially increasing the flux to form the vdW complex by a factor of two increases the R1a rate constant by at most 26%. Artificially decreasing the flux from the vdW complex to NH_2OOH by a factor of two only increases the R1a rate constant by 3% or less. Completely ignoring tunneling correlates with at most a 29% reduction in the R1a rate constant. All of these effects decrease with increasing temperature. It is perhaps worth noting that all of these parameter variations significantly exceed our best estimate of their uncertainties. Employing instead our best estimated parameter uncertainties would yield about a factor of two smaller R1a rate variations, i.e. to about 15% or less in each case.

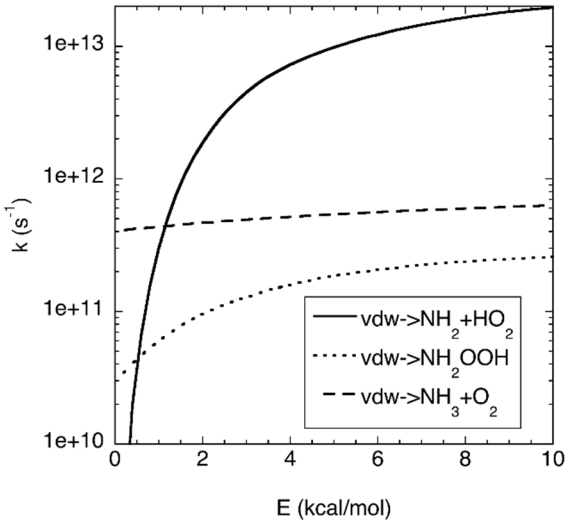

Fig. 5. Plot of the energy dependence of the rate constants for dissociation from the vdW complex. The NH_2 + HO_2 asymptote is taken as the zero of energy.

The relatively small variation of the R1a rate constant with these parameter variations is a result of the complex interplay between the various fluxes entering and exiting the vdW complex (cf. Fig. 5). For energies below the NH_2 + HO_2 asymptote, the vdW dissocation rates are irrelevant as the collision rates are not sufficient to interfere with dissociation. The insensitivity to the NH_3 + O_2 saddle point energy is related to the flatness of the corresponding microcanonical rate (dashed line), which in turn is due to its significantly submerged saddle point (-5.01 kcal/mol relative to the NH_2 + HO_2 asymptote.) The insensitivity to the entrance flux is due to the rapidity of the transition to a situation where the back dissociation dominates the vdW dissociation (i.e., the

steepness of the solid line). The insensitivity to the rate to form NH_2OOH is because this rate is always well below that for the triplet abstraction.

The ratio of the Stagni et al. predictions for the reverse $NH_3 + O_2 = NH_2 + HO_2$ rate constant (which is the direction they consider) to those from the present work are plotted in Fig. 6. In that direction, their predicted saddle point is at 52.8 kcal/mol, whereas ours is at 53.1 kcal/mol. Furthermore, their endothermicity is 57.1 kcal/mol, whereas ours is 58.1 kcal/mol. As a result, we predict somewhat smaller rate constants. At low temperature the 1 kcal/mol difference in the predicted endothermicity, which determines the flux from the vdW complex to separated $NH_2 + HO_2$, yields a significantly different reaction rate, with that difference rapidly decreasing at higher temperature. At the higher temperatures, it is remarkable how similar the two predictions are.

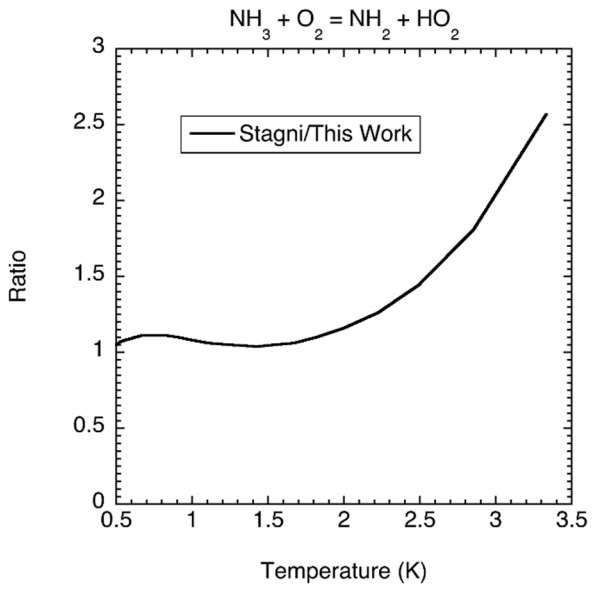

Fig. 6. Plot of the temperature dependence of the ratio of the predictions from Stagni et al. [32] to that from the present work for the reverse of reaction (R1a).

The predicted branching ratio, which is illustrated in Fig. 7, is in accord with the conclusions from the reanalysis of Glarborg et al. [24]. Notably, there is very little temperature dependence to the predicted branching ratio.

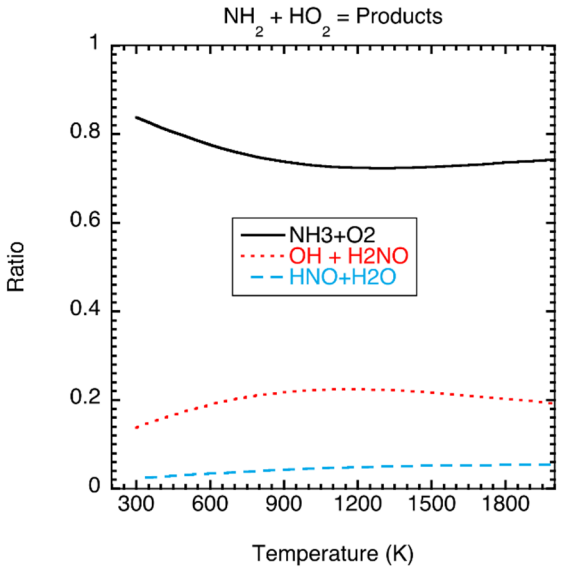

Fig. 7. Theoretically predicted branching between channels (R1a), (R1b), and (R1c).

Implications for modeling NH_3 ignition and oxidation

As discussed in the Introduction, it is important to establish reliable chemical kinetic models for ignition and oxidation of ammonia to facilitate its use in engines and gas turbines. While properties such as flame speeds can be predicted adequately with a short mechanism omitting the $NH_2 + HO_2$ reaction [56], calculations of ignition and oxidation at high pressure and intermediate temperatures are sensitive to the rate constant and branching ratio for R1 [5, 6, 57]. Most published models for NH_3 oxidation, e.g., [5, 6, 25, 56, 58-62], have relied on the theoretical work of Sumathi and Peyerimhoff [28], implying that the dominant product channel was $NH_2O + OH$ (R1c).

In their recent comprehensive modeling work, Stagni et al. [32] used their ab initio rate constant for $NH_3 + O_2$ (reverse of R1a), together with the low temperature recommendation of Baulch et al. [63] for reaction R1c, assuming it to be independent of temperature. As a result, the chain terminating channel $NH_2 + HO_2 \rightarrow NH_3 + O_2$ (R1a) becomes the dominating channel, even though its importance decreases with increasing temperature compared to $NH_2 + HO_2 \rightarrow H_2NO + OH$ (R1c).

Tests of reaction mechanisms have shown that a good prediction of ignition delays for ammonia can be achieved, independent of whether R1a or R1c are the dominant product channel for $NH_2 + HO_2$. Kawka et al. [64] tested published reaction mechanisms for NH_3 against a wide range of shock tube ignition delay data and found several models to perform well; in particular those of Shrestha et al. [61] and Glarborg et al. [25] (R1c dominant). In the review of Valera-Medina et al. [4], it was concluded that the mechanisms of both Stagni et al. [32] (R1a dominant) and Glarborg et al. [25] (R1c dominant) performed well in predicting ignition delays from shock tubes and rapid compression machines for ammonia. However, Dai et al. [57] concluded that a fast chain-terminating product channel for $NH_2 + HO_2$ was required to adequately predict ignition delays for DME/NH_3 mixtures in an RCM, and they adopted the rate constants of Stagni et al. for $NH_2 +$

HO_2. The presence of DME shifts the ignition of NH_3 to much lower temperatures than observed for pure NH_3; i.e., into a regime where the HO_2 radical has increased importance.

Here, we evaluate the impact of the choice of rate constant and branching ratio for $NH_2 + HO_2$ for prediction of ignition delays and post-ignition oxidation rate of NH_3/O_2/inert mixtures. Fig. 8 shows the predicted ignition delay times for a stoichiometric NH_3/air mixture at 100 atm with rate constants for the $NH_2 + HO_2$ reaction from Sumathi and Peyerimhoff [28], Stagni et al. [32], and the present work, respectively. The calculations were conducted with the chemical kinetic model from Glarborg et al. [25].

The predictions with the rate constants for R1 from Stagni et al. and from the present work agree within a factor of two over the range of temperature studied (900-1700 K), while the calculated ignition delay time using the rate constants from Sumathi and Peyerimhoff is up to a factor of six shorter. As expected, the differences are most pronounced at the lower temperatures, where the HO_2 radical plays a larger role in the ignition chemistry.

Fig. 9 compares predicted NH_3 consumption profiles in an atmospheric pressure flow reactor with the measurements of Dean and Lyon [65]. Similar to what was observed for the ignition delays in Fig. 8, the choice of rate parameters for the $NH_2 + HO_2$ reaction has a significant impact on predictions. If the propagating $H_2NO + OH$ channel (R1c) is dominating, as proposed by Sumathi and Peyerimhoff, the oxidation rate for ammonia is strongly overpredicted. Use of the rate constants from Stagni et al. or from the present work results in a better agreement with experiment, even though the NH_3 consumption rate is still overpredicted.

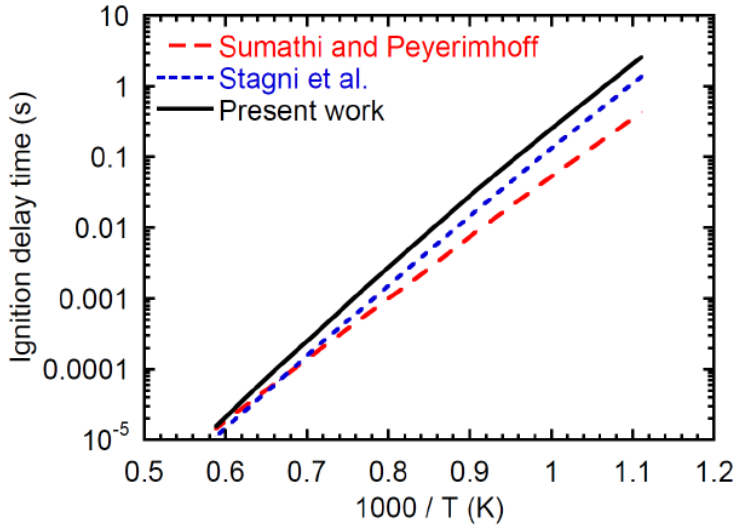

Fig. 8: Predicted ignition delay times for a stoichiometric NH_3/air mixture at 100 atm: impact of the choice of rate coefficients for $NH_2 + HO_2$. The calculations are conducted with the chemical kinetic model from Glarborg et al. [25], with rate constants for the $NH_2 + HO_2$ reaction from Sumathi and Peyerimhoff [28], Stagni et al. [32], and the present work, respectively.

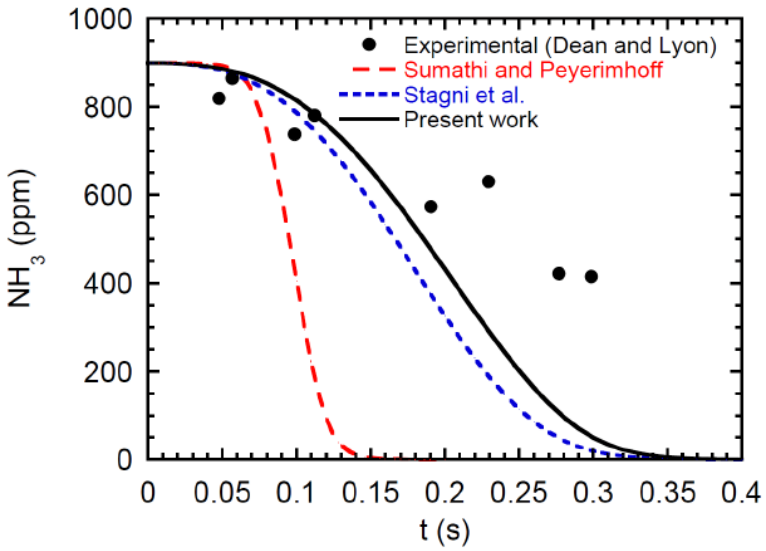

Fig. 9: Predicted and measured [65] NH_3 profiles as a function of time in a flow reactor. The calculations are conducted with the chemical kinetic model from Glarborg et al. [25], with rate constants for the $NH_2 + HO_2$ reaction from Sumathi and Peyerimhoff [28], Stagni et al. [32], and the present work, respectively. Conditions: T = 1279 K; P = 1 atm; inlet composition: 900 ppm NH_3, 4% O_2, 1% H_2O, balance N_2.

4. Conclusions

The present analysis employed a combination of high level electronic structure and transition state theory methods to obtain high accuracy predictions for the kinetics of the reaction channels of relevance to the reaction of NH_2 with HO_2. Inclusion of these rate predictions in our previously published model for nitrogen chemistry [25] has a signification impact on NH_3 ignition and oxidation.

Acknowledgements

This material is based on work supported by the U.S. Department of Energy, Office of Science, Office of Basic Energy Sciences, Division of Chemical Sciences, Geosciences, and Biosciences under contract No. DE-AC02-06CH11357. The theoretical calculations were performed by SJK with support from the Gas-Phase Chemical Physics Program.

Supplementary Material

The mess input files for the present kinetics calculations are provided in the supplementary material.

References

[1] A. Hayakawa, T. Goto, R. Mimoto, Y. Arakawa, T. Kudo, H. Kobayashi. Laminar Burning Velocity and Markstein Length of Ammonia/Air Premixed Flames at Various Pressures, Fuel, 159 (2015) 98-106.

[2] A. Valera-Medina, H. Xiao, M. Owen-Jones, W.I.F. David, P.J. Bowen, Ammonia for Power, Prog. Energy Combust. Sci. 69 (2018) 63-102.

[3] H. Kobayashi, A. Hayakawa, K.K.A. Somarathne, E.C. Okafor, Science and Technology of Ammonia Combustion, Proc. Combust. Inst. 37 (2019) 109-133.

[4] A. Valera-Medina, F. Amer-Hatem, A.K. Azad, I. Dedoussi, M. De Joannon, R.X. Fernandes, P. Glarborg, H. Hashemi, X. He, S. Mashurk, J. McGowan, C. Mounaim-Rouselle, A. Ortiz-Prado, J.A. Ortiz-Valera, I. Rossetti, B. Shu, M. Yehia, H. Xiao, M. Costa, A Review on Ammonia as a Potential Fuel: From Synthesis to Economics, Energy Fuels 35 (2021) 6964-7029.

[5] Y. Song, H. Hashemi, J.M. Christensen, C. Zou, P. Marshall, P. Glarborg, Ammonia Oxidation at High Pressure, Fuel 181 (2016) 358-365.

[6] L. Dai, S. Gersen, P. Glarborg, H. Levinsky, A. Mokhov, Experimental and Numerical Analysis of the Autoignition Behavior of NH_3 and NH_3/H_2 mixtures at High Pressure, Combust. Flame, 215 (2020) 134-144.

[7] H. Gesser. The Photolysis of Ammonia in the Presence of Propane and Oxygen, J. Amer. Chem. Soc. 77 (1955) 2626-2629.

[8] D. Husain, R.G.W. Norrish, The Explosive Oxidation of Ammonia and Hydrazine Studied by Kinetic Spectroscopy, Proc. Roy. Soc. London. Ser. A. Math. Phys. Sci. 273 (1963) 145-164.

[9] R.K.M. Jayanty, R. Simonaitis, J. Heicklen, Reaction of NH_2 with NO and O_2, J. Phys. Chem. 80 (1976) 433-437.

[10] R. Lesclaux, M. Demissy. On the Reaction of NH_2 Radical with Oxygen, Nouv. J. Chim. 1 (1977) 443.

[11] S.G. Cheskis, O.M. Sarkisov, Flash Photolysis of Ammonia in the Presence of Oxygen, Chem. Phys. Letts. 62 (1979) 72-76.

[12] V. A. Nadtochenko, O. M. Sarkisov, S. G. Cheskis. A Possible Mechanism of the Photooxidation of Ammonia, Russ. Chem. Bull. 28 (1979) 650.

[13] V.A. Lozovksii, V.A. Nadtochenko, O.M. Sarkisov, S.G. Cheskis, Study of NH_2 Radical Recombination by Intraresonator Laser Spectroscopy, Kinet. Catal. 20 (1979) 918-922.

[14] V. A. Lozovsky, S. V. Ryabchuk, O. M. Sarkisov, S. G. Cheskis, Mechanism of Ammonia Photooxidation, Khim. Fiz. 1 (1982) 113-120.

[15] R. Lesclaux, Reactivity and Kinetic Properties of the NH_2 Radical in the Gas Phase, Rev. Chem. Inter. 5 (1984) 347-392.

[16] O.M. Sarkisov, S. Cheskis, V.A. Nadtochenko, E.A. Sviridenkov, V.I. Vedeneev, Spectroscopic Study of Elementary Reactions Involving Oxomethyl, Amidogen, and Nitrosyl Hydride, Arch. Combust. 4 (1984) 111-120.

[17] R. Patrick, D. M Golden. Kinetics of the Reactions of Amidogen Radicals with Ozone and Molecular Oxygen. J. Phys. Chem. 88 (1984) 491-495.

[18] V.A. Lozovsky, M.A. Ioffe, O.M. Sarkisov, On the Reaction of the NH_2 Radical with Oxygen, Chem. Phys. Lett. 110 (1984) 651-654.

[19] J.V. Michael, R.B. Klemm, W.D. Brobst, S.R. Bosco, D.F. Nava, Flash Photolysis-Laser Induced Fluorescence Study of the Rate Constant for Amidogen (NH_2) + Molecular Oxygen Between 245 and 459 K, J. Phys. Chem. 89 (1985) 3335-3337.

[20] G.S. Tyndall, J.J. Orlando, K.E. Nickerson, C.A. Cantrell, J.G. Calvert, An Upper Limit for the Rate Coefficient of the Reaction of NH_2 Radicals with O_2 Using FTIR Product Analysis, J. Geophy. Res. 96 (1991) 20761-20768.
[21] V.A. Lozovsky, O.M. Sarkisov, A.G. Okhrimchuk, A.L. Enis. Upper Limit of the Rate Constant for the Reaction of NH_2 Radicals with O_2 Measured by Intracavity Dye Laser Spectroscopy, J. Adv. Chem. Phys. 16 (1997) 395-417.
[22] P.B. Pagsberg, J. Eriksen, H.C. Christensen. Pulse Radiolysis of Gaseous Ammonia-Oxygen Mixtures. J. Phys. Chem. 83 (1979) 582-590.
[23] O. Tokunaga, T. Sekine, M. Sakanoue, N. Suzuki, Radiolysis of Ammonia in Nitrogen; Effects of Nitrogen Monoxide and Oxygen on Decomposition of Ammonia, Int. J. Appl. Radiation Isotopes, 32 (1981) 567-572.
[24] P. Glarborg, H. Hashemi, S. Cheskis, A.W. Jasper, On the Rate Constant for $NH_2 + HO_2$ and Third Body Collision Efficiencies for $NH_2 + H$ (+M) and $NH_2 + NH_2$ (+M), J. Phys. Chem. A 125 (2021) 1505-1516.
[25] P. Glarborg, J.A. Miller, B. Ruscic, S.J. Klippenstein, Modeling Nitrogen Chemistry in Combustion, Prog. Energy Combust. Sci. 67 (2018) 31-68.
[26] C. Pouchan, B. Lam, D.M. Bishop, A Theoretical Study of the Reaction Between NH_2 and HO_2, J. Phys. Chem. 91 (1987) 4809-4813.
[27] J.W. Bozelli, A.M. Dean, Energized Complex Quantum Rice-Ramsperger-Kassel Analysis on Reactions of NH_2 with HO_2, O_2, and O Atoms, J. Phys. Chem. 93 (1989) 1058-1065.
[28] R. Sumathi, S.D. Peyerimhoff, A Quantum Statistical Analysis of the Rate Constant for the $HO_2 + NH_2$ Reaction, Chem. Phys. Letts. 263 (1996) 742-748.
[29] A.M. Dean, J.W. Bozzelli. Combustion Chemistry of Nitrogen, In W.C. Gardiner, Ed., Gas Phase Combustion Chemistry, Ch. 2. Springer-Verlag, 2000.
[30] X. Tiancheng, S. Hongyan, H. Peilin, R. Yang, Theoretical Study on the Mechanism of the HO_2 plus NH_2 Reaction, Comp. Theor. Chem. 985 (2012) 67-71.
[31] S.H. Mousavipour, F. Keshavarz, S. Soleimanzadegan, A Theoretical Study on the Dynamics of the Gas Phase Reaction of NH_2 ($^2B_1$) with HO_2 ($^2A''$). J. Iran. Chem. Soc. 13 (2016) 1115-1124.
[32] A. Stagni, C. Cavallotti, S. Arunthanayothin, Y. Song, O. Herbinet, F. Battin-Leclerc, T. Faravelli. An Experimental, Theoretical and Kinetic-Modeling Study of the Gas-Phase Oxidation of Ammonia, Reaction Chem. Eng. 5 (2020) 696-711.
[33] S.J. Klippenstein, From Theoretical Reaction Dynamics to Chemical Modeling of Combustion, Proc. Combust. Inst. 36 (2017) 77-111.
[34] S.J. Klippenstein, L.B. Harding, B. Ruscic, Ab Initio Computations and Active Thermochemical Tables Hand in Hand: Heats of Formation of Core Combustion Species, J. Phys. Chem. A 121 (2017) 6580-6602.
[35] T. Adler, G. Knizia, H.-J. Werner, A Simple and Efficient CCSD(T)-F12 Approximation. J. Chem. Phys. 127, 221106 (2007); G. Knizia, T.B. Adler, H.-J. Werner, Simplified CCSD(T)-F12 Methods: Theory and Benchmarks, J. Chem. Phys. 130 (2009) 054104.
[36] K.A. Peterson, T.B. Adler, H.-J. Werner, Systematically Convergent Basis Sets for Explicitly Correlated Wavefunctions: The Atoms H, He, B-Ne, and Al-Ar, J. Chem. Phys. 128 (2008) 084102.
[37] D.E. Woon, T.H. Dunning, Gaussian-Basis Sets for Use in Correlated Molecular Calculations. 5. Core-Valence Basis-sets for Boron through Neon, J. Chem. Phys. 103 (1995) 4572-4585.
[38] D. Peng, M. Reiher, Exact Decoupling of the Relativistic Fock Operator, Theor. Chem. Acc. 131 (2012) 1081.

[39] S. Grimme, J. Antony, S. Ehrlich, H. Krieg, A Consistent and Accurate Ab Initio Parameterization of Density Functional Dispersion Correction (DFT-D) for the 94 elements H-Pu, J. Chem. Phys. 132 (2010) 154104.
[40] MOLPRO, version 2015.1, a package of ab initio programs, H.-J. Werner, P.J. Knowles, G. Knizia, F.R. Manby, M. Schutz, P. Celani, W. Gyorffy, D. Kats, T. Korona, R. Lindh, A. Mitrushenkov, G. Rauhut, K.R. Shamasundar, T.B. Adler, R.D. Amos, A. Bernhardsson, A. Berning, D.L. Cooper, M.J.O. Deegan, A.J. Dobbyn, F. Eckert, E. Goll, C. Hampel, A. Hesselmann, G. Hetzer, T. Hrenar, G. Jansen, C. Koppl, Y. Liu, A.W. Lloyd, R.A. Mata, A.J. May, S.J. McNicholas, W. Meyer, M.E. Mura, A. Nicklass, D.P. O'Neill, P. Palmieri, D. Peng, K. Pfluger, R. Pitzer, M. Reiher, T. Shiozaki, H. Stoll, A. J. Stone, R. Tarroni, T. Thorsteinsson, M. Wang. see http://www.molpro.net
[41] H.-J. Werner, P.J. Knowles, G. Knizia, F.R. Manby, M. Schutz, Molpro: A General-Purpose Quantum Chemistry Program Package, WIREs Comput. Mol. Sci. 2 (2012) 242-253.
[42] J.F. Stanton, J. Gauss, M.E. Harding, P.G. Szalay, with contributions from A.A. Auer, R.J. Bartlett, U. Benedikt, C. Berger, D.E. Bernholdt, Y.J. Bomble, et al., and the integral packages MOLECULE (J. Almlof, P. R. Taylor,), PROPS (P. R.Taylor,), ABACUS (T. Helgaker, H. J. Jensen, P. Jørgensen, J. Olsen,), and ECP routines by A.V. Mitin, C. van Wüllen, For the current version, see: http://www.cfour.de.
[43] MRCC, A String-Based Quantum Chemical Program Suite; written by M. Kállay, see also M.; Kállay, P. R. Surján, Higher Excitations in Coupled-Cluster Theory, J. Chem. Phys. 115 (2001) 2945-2954.
[44] M.J. Frisch, G.W. Trucks, H.B. Schlegel, G.E. Scuseria, M.A. Robb, J.R. Cheeseman, G. Scalmani, V. Barone, B. Mennucci, G. A. Petersson, et al. Gaussian 09, Revision D.01; Gaussian, Inc.: Wallingford CT, 2009.

[45] A.S. Hansen, T. Bhagde, K.B. Moore III, D.R. Moberg, A.W. Jasper, Y. Georgievskii, M.F. Vansco, S.J. Klippenstein, M.I. Lester, Watching a Hydorperoxyalkyl Radical (QOOH) Dissociate, Science (2021) in press.
[46] M.I. Lester, S.J. Klippenstein, Unimolecular Decay of Criegee Intermediates to OH Radical Products: Prompt and Thermal Decay Processes, Acc. Chem. Res. 51 (2018) 978-985.
[47] A.W. Jasper, K.M. Pelzer, J.A. Miller, E. Kamarchik, L.B. Harding, S.J. Klippenstein, Science, 346 (2014) 1212-1215.
[48] S.J. Klippenstein, C. Cavallotti, Ab Initio Kinetics for Pyrolysis and Combustion Systems, in "Mathematical Modelling of Gas-Phase Complex Reaction Systems: Pyrolysis and Combustion" edited by T. Faravelli, F. Manenti, E. Ranzi, Computer Aided Chemical Engineering, 45 (2019) 115-167.
[49] S.C. Sid Ely, S.B. Morales, J.-C. Guillemin, S.J. Klippenstein, I.R. Sims, Low Temperature Rate Coefficients for the Reaction CN + HC_3N, J. Phys. Chem. A, 117 (2013) 12155-12164.
[50] S.J. Klippenstein, Variational Optimizations in the RRKM Theory Calculations for Unimolecular Dissociations with No Reverse Barrier, J. Chem. Phys. 96 (1992) 367-371.
[51] Y. Georgievski, S.J. Klippenstein, Transition State Theory for Multichannel Addition Reactions: Multifaceted Dividing Surfaces, J. Phys. Chem. A 107 (2003) 9776-9781.
[52] S.J. Klippenstein, Y. Georgievskii, L.B. Harding, Predictive Theory for the Combination Kinetics of Two Alkyl Radicals, Phys. Chem. Chem. Phys. 8 (2006) 1133-1147.
[53] G. Ghigo, B.O. Roos, P.A. Malmqvist, A Modified Definition of the Zeroth-Order Hamiltonian in Multiconfigurational Perturbation Theory, Chem. Phys. Lett. 396 (2004) 142-149.

[54] Y. Georgievskii, S.J. Klippenstein, Long-Range Transition State Theory, J. Chem. Phys. 122 (2005) 194103.
[55] Y. Georgievskii, J. A. Miller, M. P. Burke, S. J. Klippenstein, Reformulation and Solution of the Master Equation for Multiple-Well Chemical Reactions, J. Phys. Chem. A 117 (2013) 12146-12154.
[56] Y. Jiang, A. Gruber, K. Seshadri, F. Williams. An Updated Short Chemical-Kinetic Nitrogen Mechanism for Carbon-Free Combustion Applications. Int. J. Energy Res. 44 (2019) 795-810.
[57] L. Dai, H. Hashemi, P. Glarborg, S. Gersen, P. Marshall, A. Mokhov, H. Levinsky. Ignition Delay Times of NH_3 /DME Blends at High Pressure and Low DME fraction: RCM Experiments and Simulations. Combust. Flame 227 (2021) 120-134.
[58] O. Skreiberg, P. Kilpinen, P. Glarborg, Ammonia Chemistry Under Fuel-Rich Conditions in a Flow Reactor, Combust Flame 136 (2004) 501-518.
[59] S. J. Klippenstein, L. B. Harding, P. Glarborg, J. A. Miller, The Role of NNH in NO Formation and Control, Combust. Flame 158 (2011) 774-789.
[60] O. Mathieu E. L. Petersen, Experimental and Modeling Study on the High-Temperature Oxidation of Ammonia and Related NO_x Chemistry, Combust. Flame 162 (2015) 554-570.
[61] K. P. Shrestha, L. Seidel, T. Zeuch, F. Mauss, Detailed Kinetic Mechanism for the Oxidation of Ammonia Including the Formation and Reduction of Nitrogen Oxides, Energy Fuels 32 (2018) 10202-10217.
[62] B. Mei, X. Zhang, S. Ma, M. Cui, H. Guo, Z. Cao, Y. Li, Experimental and Kinetic Modeling Investigation on the Laminar Flame Propagation of Ammonia under Oxygen Enrichment and Elevated Pressure Conditions, Combust. Flame 210 (2019) 236-246.
[63] D.L. Baulch, C.T. Bowman, C.J. Cobos, R.A. Cox, T. Just, J.A. Kerr, M.J. Pilling, D. Stocker, J. Troe, W. Tsang, R.W. Walker, J. Warnatz, Evaluated Kinetic Data for Combustion Modeling: Supplement II, J. Phys. Chem. Ref. Data 34 (2005) 757-1397.
[64] L. Kawka, G. Juhasz, M. Papp, T. Nagy, I. Gy Zsely, T. Turanyi, Comparison of Detailed Reaction Mechanisms for Homogeneous Ammonia Combustion, Phys. Chem. Chem. Phys. 234 (2020) 1329-1357.
[65] A. M. Dean, J. E. Hardy, R. K. Lyon, Kinetics and Mechanism of NH_3 Oxidation, Symp. (Int.) Combust. 19 (1982) 97-105.